

# Measurements of total and partial charge-changing cross sections for 200-400 MeV/nucleon $^{12}\text{C}$ in water and polycarbonate

T. Toshito,<sup>1,2</sup> K. Kodama,<sup>3</sup> L. Sihver,<sup>4</sup> K. Yusa,<sup>5</sup> M. Ozaki,<sup>6</sup> K. Amako,<sup>2</sup> S. Kameoka,<sup>2</sup>  
K. Murakami,<sup>2</sup> T. Sasaki,<sup>2</sup> S. Aoki,<sup>7</sup> T. Ban,<sup>8</sup> T. Fukuda,<sup>8</sup> M. Komatsu,<sup>8</sup> H. Kubota,<sup>8</sup>  
N. Naganawa,<sup>8</sup> T. Nakamura,<sup>8</sup> T. Nakano,<sup>8</sup> M. Natsume,<sup>8</sup> K. Niwa,<sup>8</sup> S. Takahashi,<sup>8</sup>  
J. Yoshida,<sup>8</sup> H. Yoshida,<sup>9</sup> M. Kanazawa,<sup>10</sup> N. Kanematsu,<sup>10</sup> M. Komori,<sup>10</sup> S. Sato,<sup>10</sup>  
M. Asai,<sup>11</sup> T. Koi,<sup>11</sup> C. Fukushima,<sup>12</sup> S. Ogawa,<sup>12</sup> M. Shibasaki,<sup>12</sup> and H. Shibuya<sup>12</sup>

<sup>1</sup>*CREST, Japan Science and Technology Agency, Kawaguchi 332-0012, Japan*

<sup>2</sup>*High Energy Accelerator Research Organization (KEK), Tsukuba 305-0801, Japan*

<sup>3</sup>*Aichi University of Education, Kariya 448-8542, Japan*

<sup>4</sup>*Chalmers University of Technology SE-412 96 Gothenburg, Sweden,  
Roanoke College, Salem, VA 24153, USA*

<sup>5</sup>*Gunma University, Maebashi 371-8510, Japan*

<sup>6</sup>*Japan Aerospace Exploration Agency (JAXA), Sagamihara 229-8510, Japan*

<sup>7</sup>*Kobe University, Kobe 657-8501, Japan*

<sup>8</sup>*Nagoya University, Nagoya 464-8602, Japan*

<sup>9</sup>*Naruto University of Education, Naruto 772-8502, Japan*

<sup>10</sup>*National Institute of Radiological Sciences (NIRS), Chiba 263-8555, Japan*

<sup>11</sup>*Stanford Linear Accelerator Center (SLAC), Stanford, CA 94309, USA*

<sup>12</sup>*Toho University, Funabashi 274-8510, Japan*

## Abstract

We have studied charged nuclear fragments produced by 200 - 400 MeV/nucleon carbon ions, interacting with water and polycarbonate, using a newly developed emulsion detector. Total and partial charge-changing cross sections for the production of B, Be, and Li fragments were measured and compared with both previously published measurements, and model predictions. This study is of importance for validating and improving carbon ion therapy treatment planning systems, and for estimating the radiological risks for personnel on space missions, since carbon is a significant component of the Galactic Cosmic Rays.

PACS numbers: 25.70.Mn, 25.75.-q

Keywords: Nuclear reaction, Nuclear emulsion, Heavy ion

## I. INTRODUCTION

To understand the fragmentation of heavy ions in high energetic nucleus-nucleus interactions is very important for many different applications, e.g., heavy ion radiotherapy [1, 2] and shielding against GCR (Galactic Cosmic Rays) and SPE (Solar Particle Events) during manned missions outside the earth magnetic field [3]. For example, carbon ions of several hundred MeV/nucleon are currently used for radiotherapy at several facilities in the world. Radiotherapy with beams of heavy ions provides highly localized dose distributions at the end of the range (called Bragg peak), and is expected to be biologically more efficient than conventional photon radiation or proton beams. However, even if the heavy ions have the advantage of giving a localized dose distribution from the primary particles, the projectile fragmentation products can cause an undesired dose beyond the Bragg peak, which cause an unwanted dose to the healthy tissues. This effect can be estimated if the charge-changing cross sections of carbon ions in tissue equivalent materials, e.g., water, is known. Knowledge of fragmentation of carbon ions is also important when estimating the radiological risks in space, since the carbon is one of the most abundant heavy ion components in GCR, and its fragmentation products can make a significant contribution to the dose given to the personnel in the space vehicles. However, the fragmentation of carbon ion is not yet fully understood. Several measurements of the charge-changing cross sections of carbon in water and tissue materials have been performed [4, 5]. If compared to the predictions of different models [6, 7, 8, 9, 10, 11], significant discrepancies are observed. Moreover, measurements of partial projectile fragmentation cross sections are scarce. More experimental data are therefore needed to better understand the fragmentation of carbon ion.

From the experimental point of view, emulsion is one of the most suitable devices for detailed characterization of the fragmentation reactions, since it has the capability of spatial resolution of micron-order and excellent multi-particle separation in nearly  $4\pi$  solid angle. Despite these advantages, this technology has not been applied in the past to a high statistic experiment because the track recognition is quite time-consuming due to the manual scanning of emulsion. However, the recent success of developing an automatic image processing system called Ultra Track Selector (UTS) [12] and an event reconstruction software package (NETSCAN) [13] improved the scanning procedure greatly. Emulsion detectors are now used as core devices for large-scale elementary particle experiments [13, 14, 15]. Taking advan-

tage of this new emulsion technique, we conducted an experiment to measure fragmentation of carbon ions at HIMAC (Heavy Ion Medical Accelerator in Chiba) at NIRS (National Institute of Radiological Sciences), Chiba, Japan. In this experiment, we constructed an emulsion detector, called Emulsion Cloud Chamber (ECC), which has the ability of three dimensional track and vertex reconstruction and charge identification for each individual track.

In this paper, we report on measurements of total and partial charge-changing cross sections for incident  $^{12}\text{C}$  beams in water and polycarbonate at energies ranging from 200 to 400 MeV/nucleon. The results are discussed and compared with previous measurements and model predictions.

## II. EXPERIMENT

### A. Emulsion Cloud Chamber

The Emulsion Cloud Chamber (ECC) was designed so that it can store information about all fragmentation reactions over the whole region where primary carbons penetrate the chamber. Schematic drawings of the ECC are shown in Fig. 1. The ECC has 65 layers<sup>1</sup> of emulsion modules and acrylic frames, and its total length is 29.1 cm long. The acrylic frame has a thickness of 2 mm and its inside was filled with de-ionized water at the exposure time. The ECC was installed in a water tank which has a window of 1-mm-thick acrylic plate on the side of beam injection.

Each emulsion module has four emulsion sheets reinforced with a 1.05-mm-thick polycarbonate ( $\text{C}_{16}\text{H}_{14}\text{O}_3$ ) plate whose measured density is  $1.16 \text{ g/cm}^3$ . A pair of emulsion sheets covers on both sides of the plate as shown in Fig. 1(b).<sup>2</sup> The polycarbonate plate keeps the flatness of the emulsion module, though it was also used as a target material. Each emulsion module is vacuum-packed with an aluminum-coated film for light and water shielding. The OPERA film [16] - a nuclear emulsion film developed for the OPERA experiment [15], was used as the emulsion sheet. An OPERA film measures 102 mm by 127 mm and has  $44\text{-}\mu\text{m}$ -thick emulsion layers coated on both sides of a  $205\text{-}\mu\text{m}$ -thick TAC (cellulose triacetate) base

---

<sup>1</sup> Consecutive numbers are assigned to the layers along the beam direction.

<sup>2</sup> The labels “A” to “D” are assigned to emulsion sheets in each module as shown in Fig. 1(b).

as shown in Fig. 1(c).

## B. Beam exposure and development

The beam exposure was performed in the SB2 beam line [17] of the HIMAC heavy ion synchrotron in December 2004. The primary  $^{12}\text{C}$  beam with a kinetic energy of 400 MeV/nucleon was extracted to the beam line and directly delivered to the experimental area.

The beam size and intensity were optimized so that the surface of ECC corresponding to the scanning area ( $12.5\text{ cm}^2$ ) was irradiated uniformly with a proper density. Beam density is one of the most critical parameters for the exposure, and exposures at excessive densities cause overlapping of particles, which makes the track reconstruction difficult. We controlled the beam density to be of the order of  $10^3$  particles/ $\text{cm}^2$  which is the optimal density to observe fragmentation reactions at energies above 200 MeV/nucleon. We placed a 1-mm-thick plastic scintillator between the end of the beam pipe and the ECC, to monitor the number of injected charged particles. The total count of beam tracks was 23874, and the beam density was measured to be  $1.6 \times 10^3$  particles/ $\text{cm}^2$ . The purity of  $^{12}\text{C}$  of the beam at the front of the ECC was estimated to be 99.5% by taking into account the interactions of  $^{12}\text{C}$  in the materials between the vacuum beam pipe and the ECC.

After the exposure, the emulsion sheets were shipped to the scanning facility at Nagoya University. Sheets-A and C were developed normally and sheets-B and D were processed applying so-called the refreshing method [18] before development. Refreshing is a technology to erase minimum ionizing tracks in emulsion by means of forced fading under a high temperature and high humidity environment. It desensitizes emulsion and extends the dynamic range of response to highly charged particles. In Ref. [18] we showed that charges of ion tracks can be identified up to  $Z = 6$  with the refreshing method. Sheets-B and D were refreshed for three days under the temperatures of  $40\text{ }^\circ\text{C}$  and  $38\text{ }^\circ\text{C}$  respectively and the relative humidity of 98%.

### III. ANALYSIS

#### A. Emulsion read-out

We used the UTS (Ultra Track Selector) [12] to read out track images in the emulsion films. UTS takes 16 layers of tomographic CCD images from a 44- $\mu\text{m}$ -thick emulsion layer of a film. The imaging processor of UTS automatically finds track segments in an emulsion layer as three dimensional vectors. The UTS system has the field view of 150  $\mu\text{m}$  by 120  $\mu\text{m}$  and processes three views per second. Track segments with the tangents of the polar angles less than 0.5 were recorded, and the detection efficiency of a track segment was 98%. After the scanning, two corresponding track segments in the emulsion layers of both sides were connected across the TAC base, a new track segment was thus created. This is called a base track. The positional and angular resolutions of a base track were found to be 1  $\mu\text{m}$  and 6 mrad, respectively.

UTS also records the grain density of a track segment, which keeps information on the local energy deposited. The grain density is digitized to pixel counts of CCD images whose pixel size is 0.29  $\mu\text{m}$  by 0.23  $\mu\text{m}$ . The pulse height is defined as the total pixel counts along each base track and used to identify a track charge at the later stage.

#### B. Track and vertex reconstruction

The NETSCAN software framework [13] was utilized for track and vertex reconstruction. NETSCAN reconstructs trajectories of charged particles by connecting base tracks which lay within a certain distance. At the tracking stage, only base tracks in sheets-A were used. The probability of misconnection of two base tracks in adjacent modules was expected to be less than 1% for the primary beam tracks. The base tracks in sheets-B and D, which were desensitized with the refreshing method, were matched and associated with each reconstructed track.

After the track reconstruction, the three dimensional vertex reconstruction was performed. Tracks starting inside the ECC and having a certain distance from a beam particle were selected as secondaries. Then, the vertex position was calculated searching for the position at which multiple tracks converged. We also imposed that an impact parameter of each secondary track should be less than 20  $\mu\text{m}$ , which was determined to associate the

secondary tracks having the energy above 200 MeV/nucleon with a correct vertex at more than 99% efficiency by considering the effect of multiple coulomb scattering. The position resolution of a vertex was found to be 50  $\mu\text{m}$  in the beam direction.

### C. Charge identification

Pulse height information was used to identify the charge of each track. Figure 2 shows the pulse height distribution for secondary tracks, where the pulse heights are averaged among the connected base tracks in non-refreshing films of Sheets-A. As seen in the figure, pulse heights for multiple charged tracks overlap with each other and the track charges cannot be distinguished by this data alone. We therefore determined the track charges in two steps. At a first step, single charged tracks were discriminated from multiple charged tracks, demanding that the averaged pulse heights are less than 210 as shown in Fig. 2. We estimated that 6% of single charged tracks were misidentified as multiple charged tracks by this separation. Then, as a second step, we used pulse height information of refreshed films. The refreshing method desensitizes the emulsion films and decreases the pulse heights depending on refresh conditions. Sheets-B and sheets-D were refreshed in different conditions, so that they would show different responses to ion charges. Figure 3 presents a scatter plot between pulse heights averaged in sheets-B and sheets-D for secondary tracks. Clear discrimination of track charges from  $Z = 2$  to  $Z = 6$  can be obtained as seen in the figure. Likelihood analysis was applied for actual charge determination. The likelihood function is defined as

$$L(Z) \equiv \prod_{i=B,D} P_i(Z, x),$$

where  $P_i(Z, x)$  is the probability function of a pulse height ( $x$ ) for a specific charge ( $Z$ ) and a refresh condition ( $i$ ). We assumed that the pulse height distributions were Gaussian, where the mean pulse height and its deviation for individual charge were estimated by measured values for each refresh condition. Finally, the track charges were determined by varying the  $Z$  from two to six and finding the value which gave the maximum of the above likelihood function. The separation between  $Z = 5$  and  $Z = 6$  is most crucial, and the misidentification probability was estimated from the breadth of the pulse height distributions and found to be 1.4%.

#### D. Counting of charge-changing interactions

The charge-changing interactions were identified principally by finding vertices whose primary tracks were observed as  $Z = 6$  and any of its secondary tracks were not  $Z = 6$ . To ensure beam tracks, primary tracks were also required to be connected from the uppermost module. However a certain number of charge-changing interactions were missed using this identification condition. For instance, if a primary carbon and a secondary track were reconstructed as a single straight track, then the vertex would not be found. The following case is conceivable; a primary carbon changes to a secondary fragment with a kink angle too small to detect and no other secondary tracks are found in the angular acceptance ( $\tan\theta < 0.5$ ). In order to recover these kinds of events, pulse height variations were traced along primary carbon tracks. Figure 4 shows an example of this type of track (we call it a “charge-changing track”). As seen in the figure, a charge-changing interaction can be detected as a discrete change of pulse heights like a step function. It turned out that 87% of the interactions were detected as reconstructed vertices and the rest were counted as charge-changing tracks.

For reconstructed vertices, we can recognize carbon-water and carbon-polycarbonate interactions by the vertex positions. Figure 5 shows the distribution of local distance between the surface of each module and reconstructed vertices (also see Fig. 1(b)). The target materials of interactions were identified according to the detector structure as shown in the figure. For charge-changing tracks, we cannot directly determine the target material, because we cannot get the exact vertex position. To evaluate the number of interactions, we did the following. The number of interactions,  $N_T(i)$ , in a target material of  $T$  (water or polycarbonate) of  $i$ -th module can be obtained by

$$N_T(i) = N_T^{rec}(i) + R_T N^{cct}(i),$$

where  $N_T^{rec}$  denotes the number of reconstructed vertices in a target ( $T$ ) and  $N^{cct}$  is the number of charge-changing tracks. Here  $R_T$  is introduced as the ratio of reactions in water or polycarbonate to those in the whole region of the ECC.<sup>3</sup> The ratio was given for each

---

<sup>3</sup> In Fig. 5, one can see a deterioration in vertex reconstruction at the first emulsion layer. This is due to interactions inside the emulsion layers which were used for tracking. Actual counts of interactions in the first emulsion region were taken as those in the second region.



charge-changing;  $\Delta Z = 1, 2, 3, 4,$  and  $5$ . The counting inefficiency due to problems in reconstruction of secondary particles was estimated to be less than 2%.

In the lower energy region, the track and vertex reconstruction deteriorates due to larger scattering. As effective events, we analyzed interactions in the upstream modules from 35th module, which corresponds to the beam energy above 200 MeV/nucleon. Finally, we obtained 8213 interactions in this region of the ECC.

## IV. RESULTS AND DISCUSSION

### A. Total charge-changing cross section

The total charge-changing cross section ( $\sigma_{tot}$ ) for a target material  $T$  in  $i$ -th module can be approximated by

$$\sigma_{tot}(i) = \frac{M}{N_A \rho t} \frac{N_T(i)}{N_C(i)},$$

where  $N_A$  is Avogadro's number,  $M$  is the molecular mass in atomic units of the target material,  $\rho$  is the target mass density,  $t$  is the target thickness, and  $N_C(i)$  is the number of primary carbon tracks impinging on  $i$ -th module. To reduce statistical errors, successive five (ten) modules are combined for carbon-water (carbon-polycarbonate) interactions. In Figs. 6 and 7 our measured total charge-changing cross sections, from the interactions of carbon with water and polycarbonate, are plotted together with measurements from Ref. [4] and Ref. [5]. These cross sections and their statistical errors are also listed in Tables I and II. The cross sections of the carbon-polycarbonate (C-C<sub>16</sub>H<sub>14</sub>O<sub>3</sub>) reactions in the references are obtained from the combination of cross sections in different target materials; carbon-carbon (C-C), carbon-paraffin (C-CH<sub>2</sub>), and carbon-water (C-H<sub>2</sub>O) interactions. The beam energy at each module was estimated by energy loss calculation using Geant4 [19]. As can be seen, our measurements agree well with the previous measurements at overlapping energies around 250 MeV/nucleon.

We have also compared our results with calculations based on the Sihver's model [6], which are superimposed in Figs. 6 and 7. Sihver's model is a semi-empirical model which takes advantage of the experimentally verified weak factorization property [20]. The model is used in the treatment planning systems for heavy ion radiotherapy at several facilities in the world. It is also used in models for calculations of Galactic Cosmic Rays, etc. As can

be seen in Figs. 6 and 7, the total charge-changing cross sections are quite consistent with the model predictions at energies above 250 MeV/nucleon, while the predictions differ from our results by about 10% in the lower energy region.

The systematic error in our measurements consists of the following components:

1. The uncertainty in vertex positions affected the position cut for selecting a target material, and resulted in an uncertainty of 3%.
2. The probability of charge misidentification of primary or secondary particles gave the uncertainty of 5%.
3. The inefficiency of counting charge-changing reactions was taken as the fractional systematic error of 2%.

The contamination of  $^{10}\text{C}$  and  $^{11}\text{C}$  in the  $^{12}\text{C}$  beam was expected to be 3%. Assuming that the differences of the cross sections between these isotopes are small, the contribution to the systematic error is considered to be negligibly small [5]. By summing up all these uncertainties, we get an estimated total systematic error of 6%.

## B. Partial charge-changing cross section

The partial projectile charge-changing cross section ( $\sigma_{\Delta Z}$ ) is defined as the cross section producing a projectile-like fragment with a specific charge difference  $\Delta Z = 6 - Z_{\text{fragment}}$ , ranging from  $\Delta Z = 1$  for B to  $\Delta Z = 5$  for protons. Figures 8-10 and 11-13 show our measurement results for carbon reactions of  $\Delta Z = 1, 2,$  and  $3$  in targets of water and polycarbonate, respectively. In Figs. 8, 9, 11, and 12, our measured partial charge-changing cross sections are also compared with the measurements published in Ref. [5]. All cross sections are also listed in Tables III and IV. As can be seen from these figures, our measurements agree well with previously performed measurements at overlapping energies around 250 MeV/nucleon.

We have also compared with calculations based on the Sihver's model [6], which are superimposed in Figs. 8-13.<sup>4</sup> The model predictions for the partial cross sections show

---

<sup>4</sup> The values of Sihver's model were obtained by summing up for all detectable isotopes with  $A = 11, 10, 8$  for  $\Delta Z = 1$ ,  $A = 10, 9, 7$  for  $\Delta Z = 2$ , and  $A = 7, 6$  for  $\Delta Z = 3$ .

stronger energy dependence than our measurements, and we found significant discrepancies, especially in the lower energy region. The deviations between the measured and the calculated cross sections for the fragments with  $\Delta Z = 1, 2,$  and  $3$  at the projectile energy  $255$  MeV/nucleon, are  $21\%$ ,  $23\%$ , and  $24\%$  for the carbon-water interactions, and  $16\%$ ,  $33\%$ , and  $4\%$  for carbon-polycarbonate interactions, respectively. The total systematic error was estimated to be  $6\%$ , in the same way for the total cross sections.

We do not present the results of the partial charge-changing cross sections for  $\Delta Z = 4$  and  $5$  i.e., the production of  $\alpha$  and  $p$ , since these light particles have energy and angular distributions beyond the detector acceptance; and contamination of light target fragments can not be neglected.

## V. CONCLUSIONS

We have measured charged nuclear fragments produced by  $200 - 400$  MeV/nucleon carbon ions, interacting with water and polycarbonate, using a newly developed emulsion technique. Both total and partial charge-changing cross sections were measured, and the results were compared with previous measurements and model predictions. The measured total charge-changing cross sections showed good agreement with both the reference measurements and simulations using a model developed by Sihver et al. [6]. In the case of the partial cross sections Sihver's model showed stronger energy dependence than our measurements, and deviated from our measurements in the lower energy region. This proves that measurements performed by our ECC can help improve and validate theoretical fragmentation models. Since  $200 - 400$  MeV/nucleon is the energy region where carbon ion therapy is performed at several facilities, our data is of importance for validating and improving the treatment planning systems. The results are also of importance when estimating the radiological risks for personnel on space missions, since carbon is a significant component of the GCR.

## ACKNOWLEDGMENTS

This research was performed as an Research Project with Heavy Ions at NIRS-HIMAC. Also this work was supported in part by CREST of Japan Science and Technology Agency (JST). We would like to thank B. Lundberg for carefully reading this paper.

- 
- [1] W.T. Chu and B.A. Ludewigt, and T.R. Renner, Rev. Sci. Instrum. **64**, 2005 (1993).
- [2] P.L. Petti and A.J. Lennox, Annu. Rev. Nucl. Part. Sci. **44**, 155 (1994).
- [3] J. Miller et al. Acta. Astronautica **42**, 389 (1998).
- [4] I. Schall et al. Nucl. Instrum. Methods B **117**, 221 (1996).
- [5] A.N. Golovchenko et al. Nucl. Instrum. Methods B **159**, 233 (1999); A.N. Golovchenko et al. Phys. Rev. C **66**, 014609 (2002).
- [6] L. Sihver, C.H. Tsao, R. Silberberg, T. Kanai, and A.F. Barghouty, Phys. Rev. C **47**, 1225 (1993); L. Sihver, D. Schardt, and T. Kanai, Jpn. J. Med. Phys. **18**, 1 (1998); L. Sihver, D. Mancusi, T. Kanai, and N. Matsufuji, "HIBRAC: a 1-D deterministic heavy-ion transport code optimised for radiotherapy", Phys. Med. Biol. (submitted 2006).
- [7] J.W. Wilson et al. Nucl. Instrum. Methods B **94**, 95 (1994); NASA TP-3533, (1995).
- [8] R.K. Tripathi, F.A. Cucinotta and J.W. Wilson, Nucl. Instrum. Methods B **117**, 347 (1996).
- [9] T. Brohm and K.-H. Schmidt, Nucl. Phys. A **569**, 821 (1994).
- [10] C.H. Tsao, R. Silberberg, A.F. Barghouty, L. Sihver, and T. Kanai, Phys. Rev. C **47**, 1257 (1993).
- [11] K. Summerer and B. Blank, Phys. Rev. C **61**, 034607 (2000).
- [12] S. Aoki et al. Nucl. Instrum. Methods B **51**, 466 (1990); T. Nakano, in Proceedings of International Workshop on Nuclear Emulsion Techniques, Nagoya, Japan, 1998; in *Proceedings of International Europhysics Conference on High Energy Physics, Budapest, Hungary, 2001*, edited by Dezso Horvath, Peter Levai, Andras Patkos.
- [13] K. Kodama et al. Nucl. Instrum. Methods A **493**, 45 (2002).
- [14] E. Eskut et al. Nucl. Instrum. Methods A **401**, 7 (1997).
- [15] M. Guler et al. OPERA experimental proposal CERN/SPSC 2000-028, SPSC/P318, LNGS P25/2000 (2000).
- [16] K. Kuwabara and S. Nishiyama, Journal of the society of photographic science and technology of Japan **67**, 521 (2004); T. Nakamura et al. Nucl. Instrum. Methods A **556**, 80 (2006).
- [17] M. Kanazawa et al. Nucl. Phys. A **746**, 393c (2004); Y. Iseki et al. Phys. Med. Biol. **49**, 3179 (2004).
- [18] T. Toshito et al. Nucl. Instrum. Methods A **556**, 482 (2006).

- [19] S. Agostinelli et al. Nucl. Instrum. Methods A **506**, 250 (2003); J. Allison et al. IEEE Trans. Nucl. Sci. **53** No.1, 270 (2006).
- [20] D. L. Olson, B. L. Berman, D. E. Greiner, H. H. Heckman, P. J. Lindstrom and H. J. Crawford, Phys. Rev. C **28**, 1602 (1983).

TABLE I: Comparison of total charge-changing cross sections of  $^{12}\text{C}$  beams in water target.

Our measurements		Ref. [4]		Ref. [5]	
E (MeV/nucleon)	$\sigma_{tot}$ (mb)	E (MeV/nucleon)	$\sigma_{tot}$ (mb)	E (MeV/nucleon)	$\sigma_{tot}$ (mb)
$377 \pm 12$	$1253 \pm 45$				
$352 \pm 13$	$1202 \pm 47$				
$326 \pm 13$	$1250 \pm 51$				
$299 \pm 14$	$1183 \pm 52$				
$271 \pm 15$	$1193 \pm 56$	$259 \pm 47$	$1205 \pm 34$		
$241 \pm 16$	$1241 \pm 61$	$241 \pm 26$	$1163 \pm 13$	$241 \pm 33$	$1191 \pm 35$
$208 \pm 17$	$1231 \pm 64$				

TABLE II: Comparison of total charge-changing cross sections of  $^{12}\text{C}$  beams in polycarbonate ( $\text{C}_{16}\text{H}_{14}\text{O}_3$ ) target. The values of Ref. [4] and Ref. [5] are obtained from the combination of cross sections in different target materials (C,  $\text{CH}_2$ , and  $\text{H}_2\text{O}$ ).

Our measurements		Ref. [4]		Ref. [5]	
E (MeV/nucleon)	$\sigma_{tot}$ (mb)	E (MeV/nucleon)	$\sigma_{tot}$ (mb)	E (MeV/nucleon)	$\sigma_{tot}$ (mb)
$364 \pm 25$	$17682 \pm 595$				
$312 \pm 27$	$16723 \pm 648$				
$255 \pm 30$	$17225 \pm 747$	$226 \pm 41$	$16765 \pm 134$	$241 \pm 33$	$17625 \pm 562$

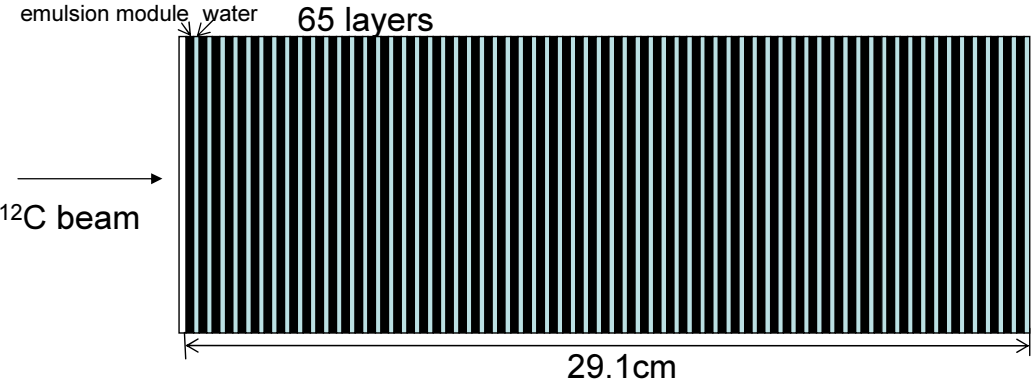
TABLE III: Comparison of partial charge-changing cross sections of  $^{12}\text{C}$  beams in water target.

$\Delta Z$	Our measurements		Ref. [5]	
	E (MeV/nucleon)	$\sigma_{\Delta Z}$ (mb)	E (MeV/nucleon)	$\sigma_{\Delta Z}$ (mb)
1	$364 \pm 25$	$221 \pm 14$		
	$312 \pm 27$	$218 \pm 15$		
	$255 \pm 30$	$210 \pm 17$	$241 \pm 33$	$210 \pm 6$
2	$364 \pm 25$	$89 \pm 9$		
	$312 \pm 27$	$95 \pm 10$		
	$255 \pm 30$	$93 \pm 11$	$241 \pm 33$	$84 \pm 4$
3	$364 \pm 25$	$120 \pm 10$		
	$312 \pm 27$	$115 \pm 11$		
	$255 \pm 30$	$128 \pm 13$		

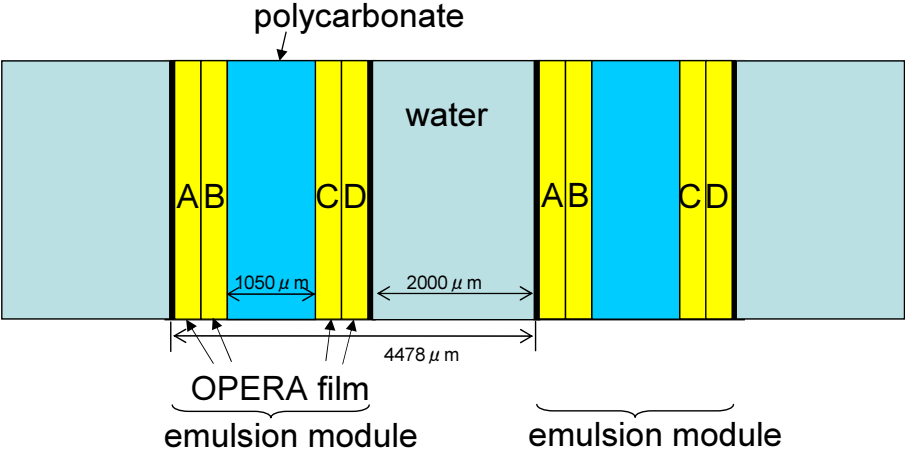
TABLE IV: Comparison of partial charge-changing cross sections of  $^{12}\text{C}$  beams in polycarbonate ( $\text{C}_{16}\text{H}_{14}\text{O}_3$ ) target. The values of Ref. [5] are obtained from the combination of cross sections in different target materials (C,  $\text{CH}_2$ , and  $\text{H}_2\text{O}$ ).

$\Delta Z$	Our measurements		Ref. [5]	
	E (MeV/nucleon)	$\sigma_{\Delta Z}$ (mb)	E (MeV/nucleon)	$\sigma_{\Delta Z}$ (mb)
1	$364 \pm 25$	$2968 \pm 243$		
	$312 \pm 27$	$3162 \pm 281$		
	$255 \pm 30$	$2714 \pm 296$	$241 \pm 33$	$2890 \pm 70$
2	$364 \pm 25$	$957 \pm 138$		
	$312 \pm 27$	$1158 \pm 170$		
	$255 \pm 30$	$1027 \pm 182$	$241 \pm 33$	$1028 \pm 43$
3	$364 \pm 25$	$1903 \pm 195$		
	$312 \pm 27$	$1798 \pm 212$		
	$255 \pm 30$	$1992 \pm 253$		

(a) ECC whole structure



(b) Detailed structure



(c) OPERA film

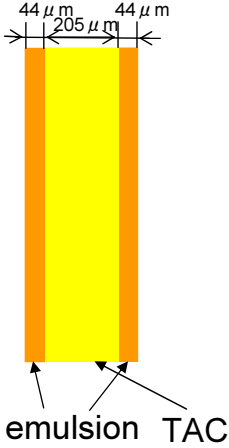


FIG. 1: (Color online) (a) A schematic view of the whole structure of the Emulsion Cloud Chamber (ECC). It has 65 layers of emulsion modules and water targets. (b) Detailed structure of the ECC. An emulsion module consists of four emulsion sheets and a polycarbonate plate. (c) Cross section of an OPERA film. An OPERA film has emulsion layers coated on both sides of a TAC base.



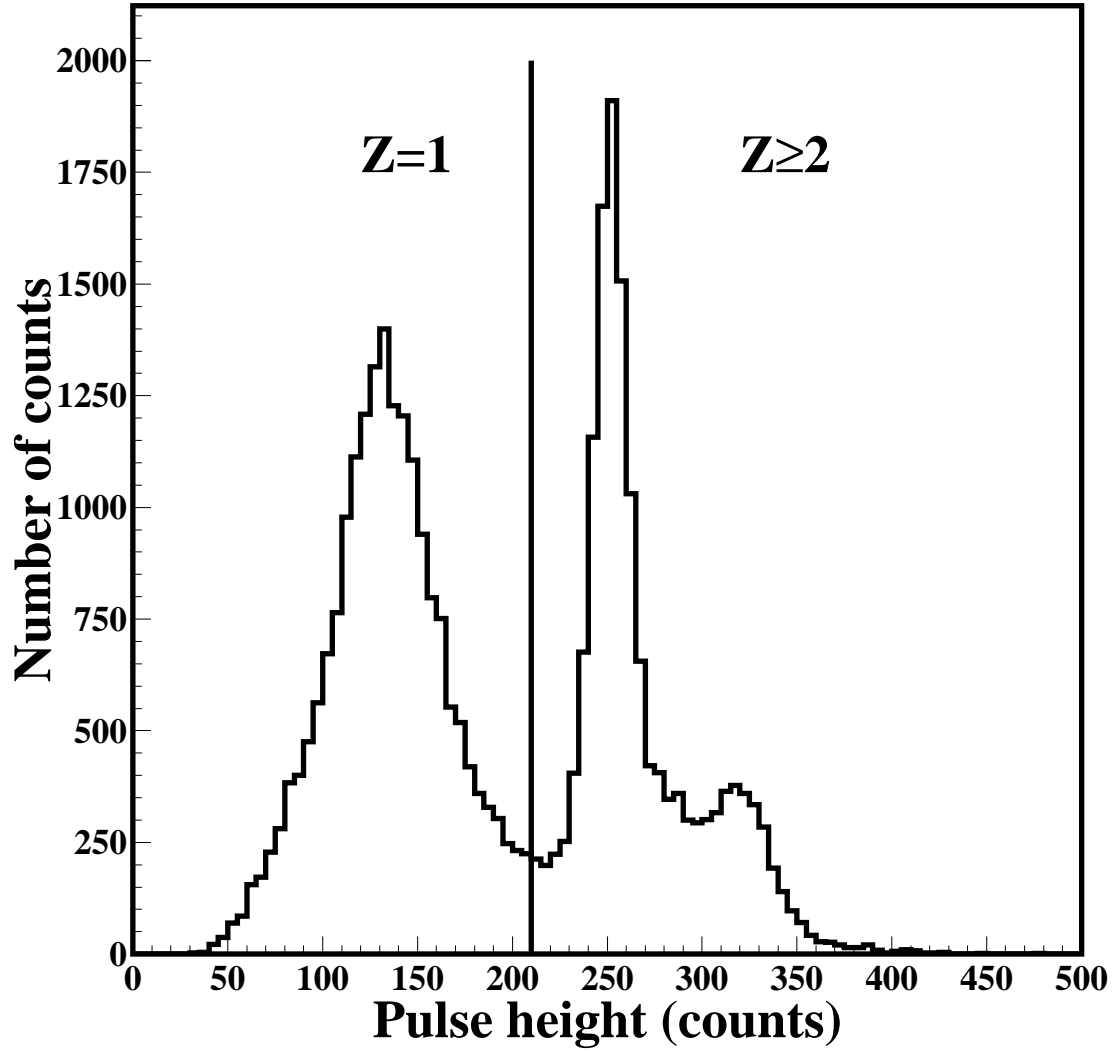


FIG. 2: Distribution of the pulse heights in sheets-A for secondary tracks. The tracks with pulse heights less than 210 are discriminated as single charged tracks.

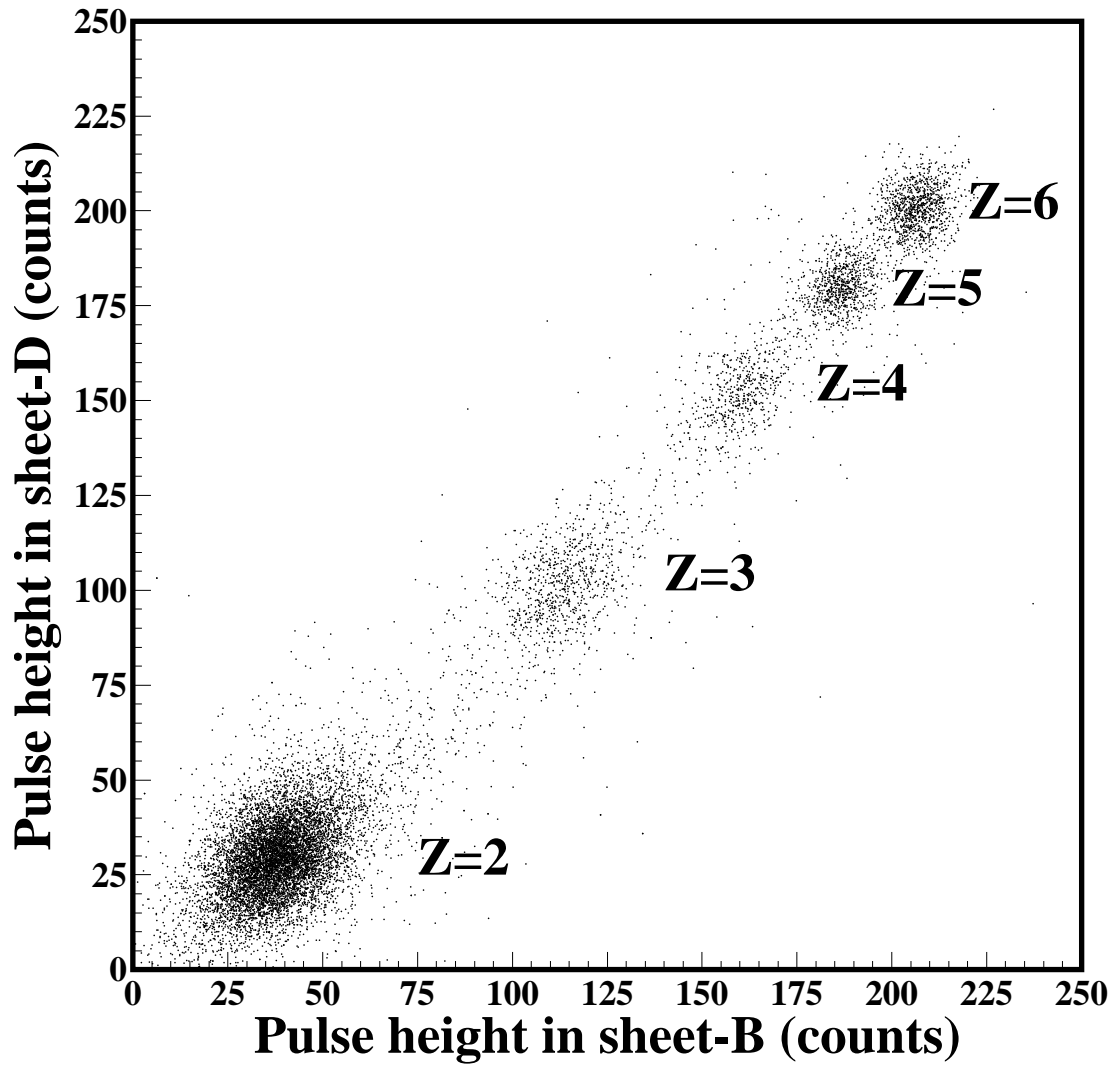


FIG. 3: A scatter plot between averaged pulse heights in sheets-B and sheets-D for secondary tracks. One can see clear discrimination of track charges from  $Z = 2$  to  $Z = 6$ .

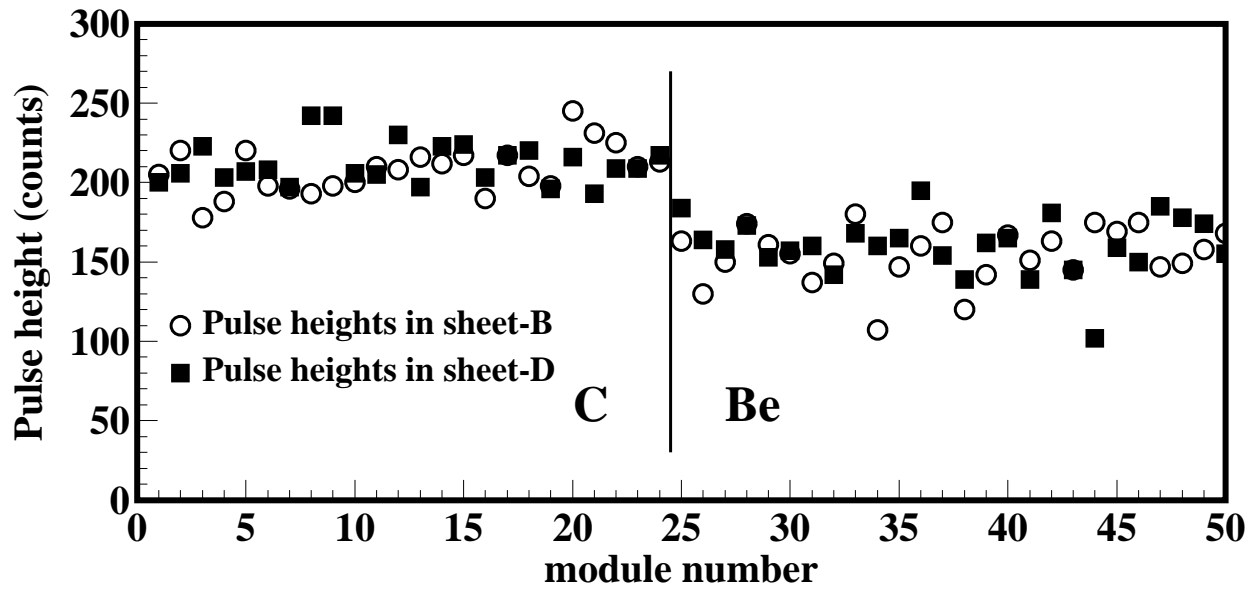


FIG. 4: An example of a charge-changing track. Open circles (Black squares) represent averaged pulse heights in sheets-B (sheets-D). We traced pulse height variations along primary carbon tracks. In this case, a carbon beam changes into a beryllium between 24th and 25th modules.

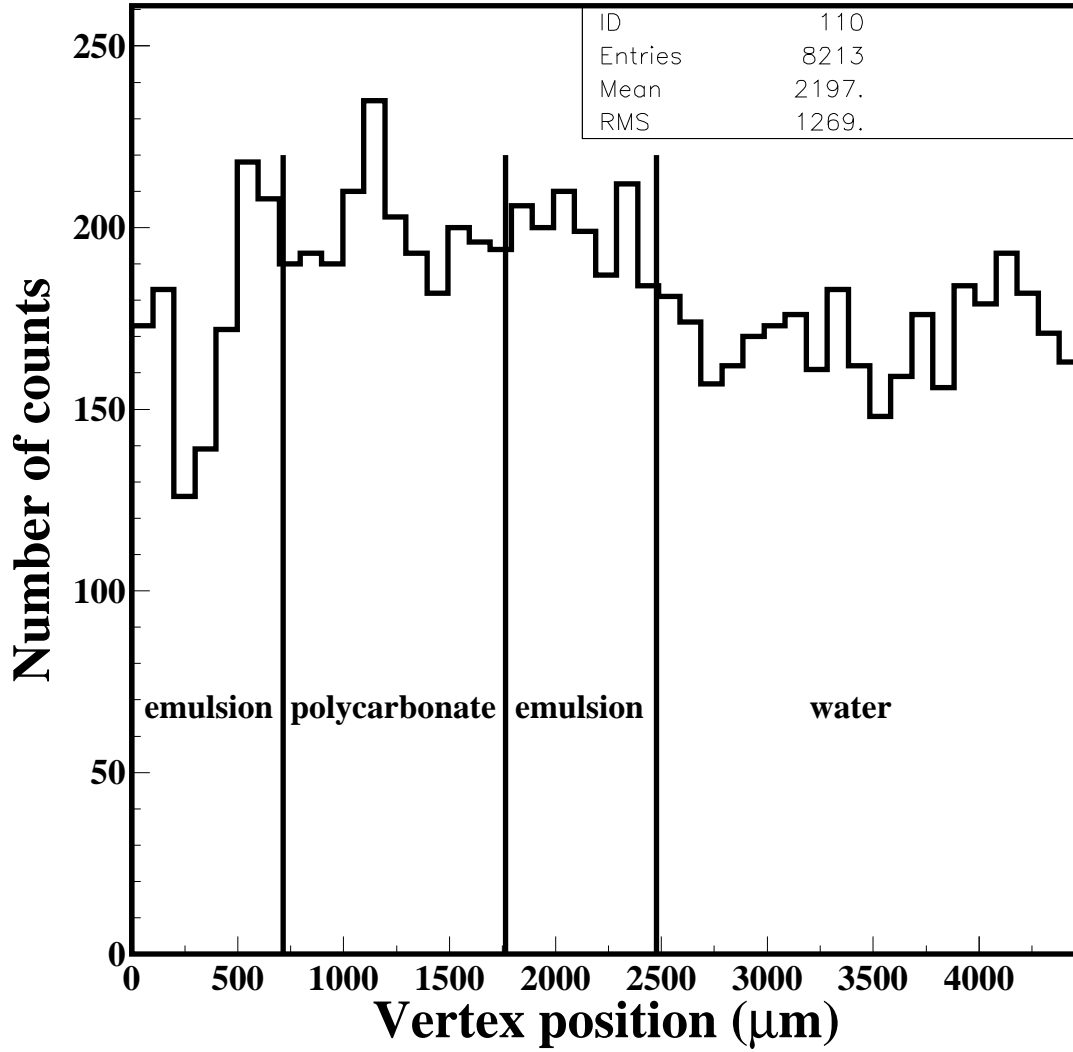


FIG. 5: Distribution of local distance between the surface of each module and reconstructed vertices. The target materials of interactions were identified according to the detector structure (also see Fig. 1(b)).

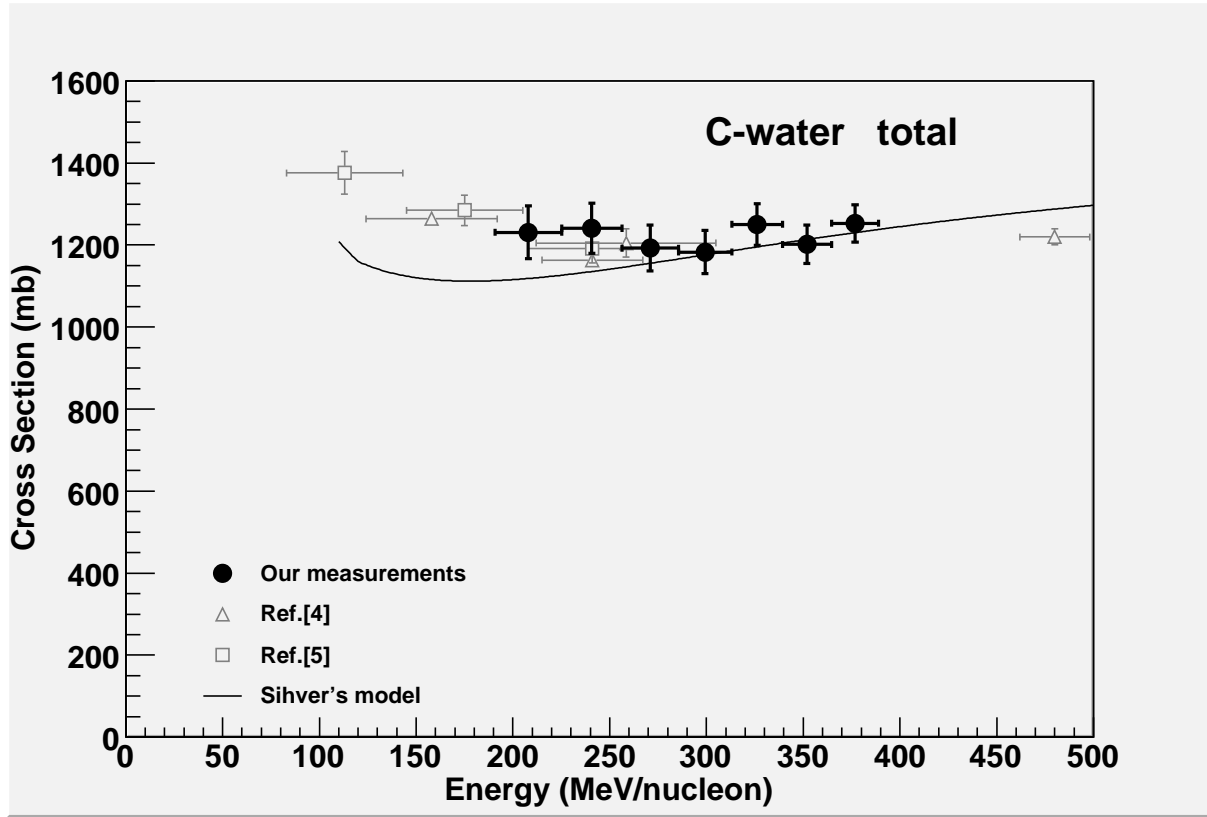


FIG. 6: Total charge-changing cross sections of carbon-water interactions in comparison with previous measurements and a model calculation. The vertical error bars indicate statistical errors only in this and the followings figures.

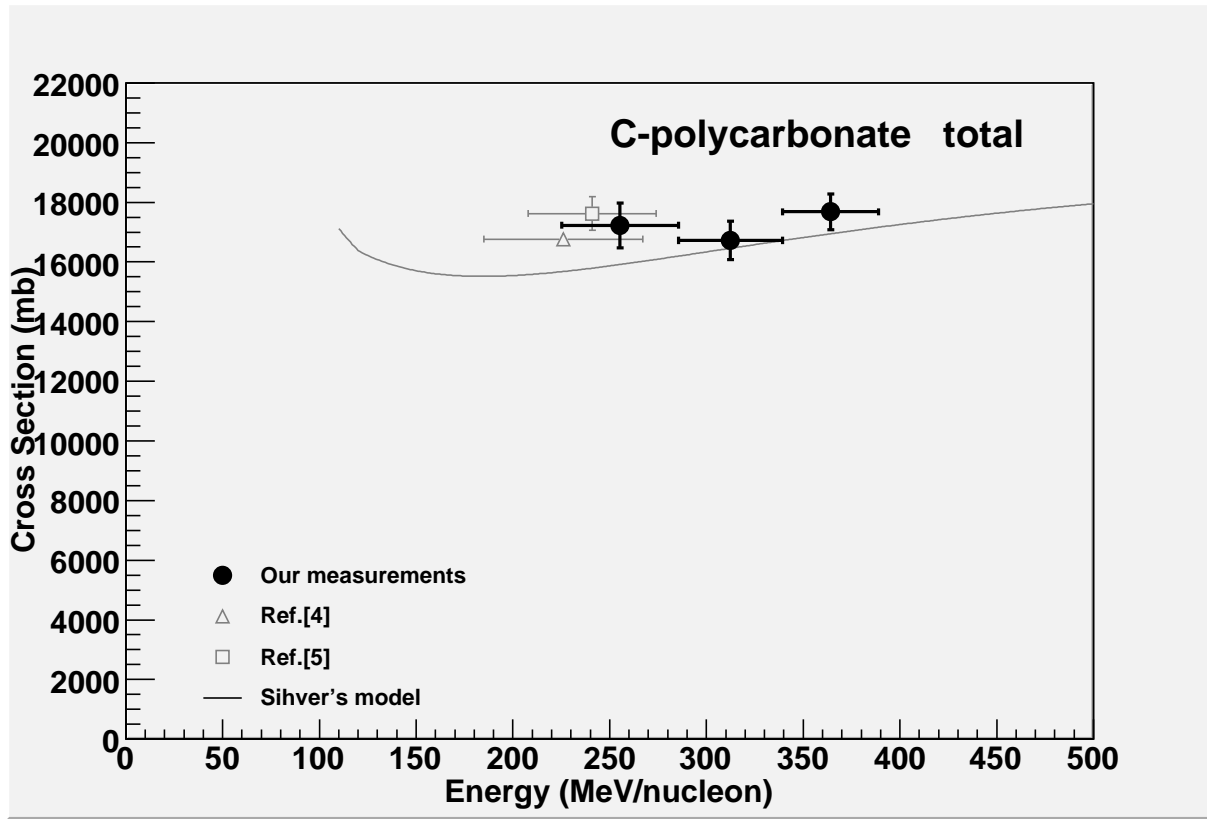


FIG. 7: Total charge-changing cross sections of carbon-polycarbonate interactions in comparison with previous measurements and a model calculation.

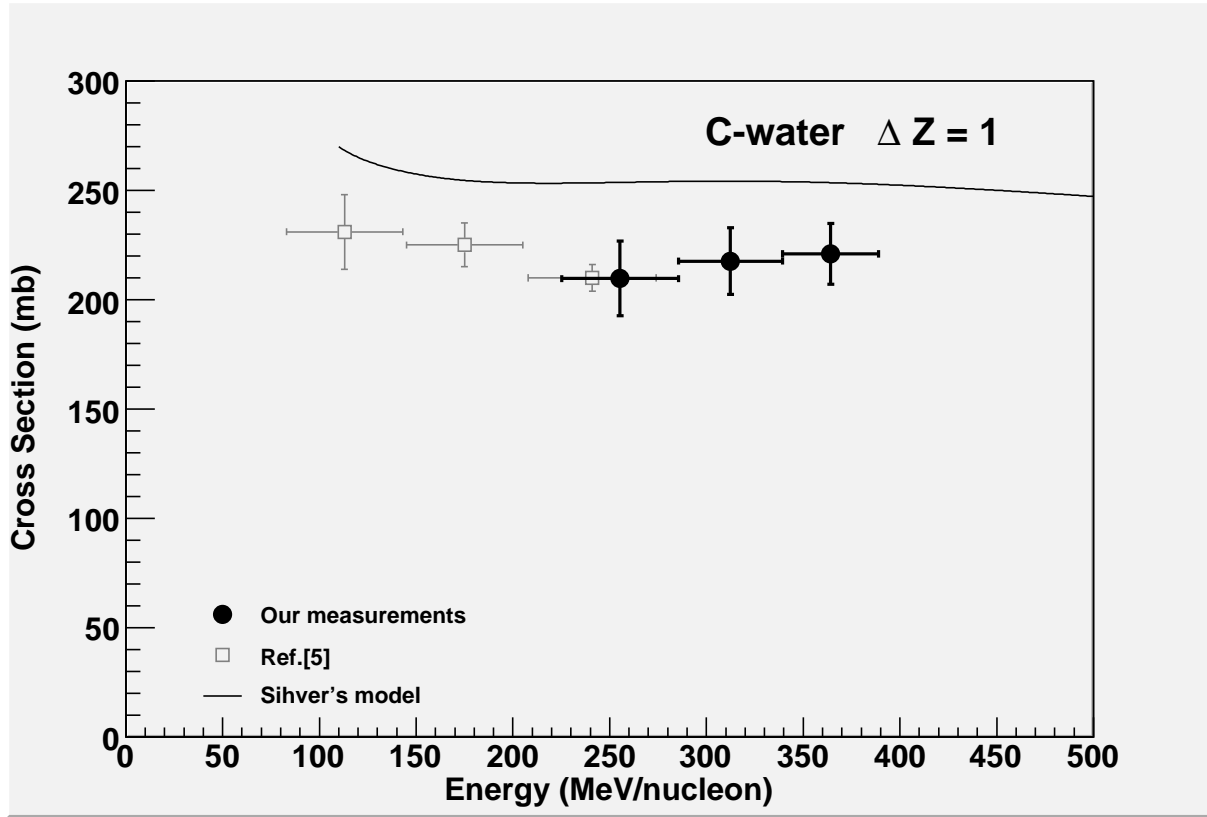


FIG. 8: Partial charge-changing cross sections of carbon-water interactions of  $\Delta Z = 1$  in comparison with previous measurements and a model calculation.

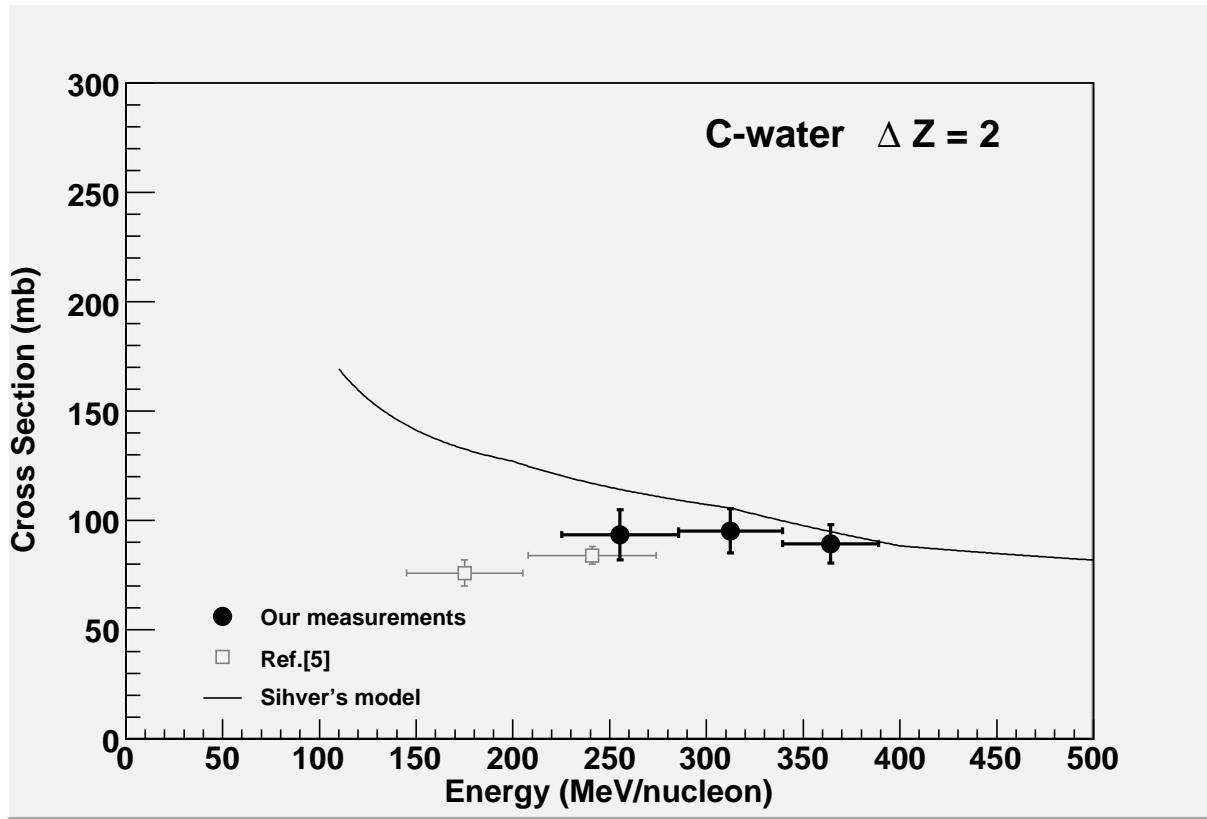


FIG. 9: Partial charge-changing cross sections of carbon-water interactions of  $\Delta Z = 2$  in comparison with previous measurements and a model calculation.



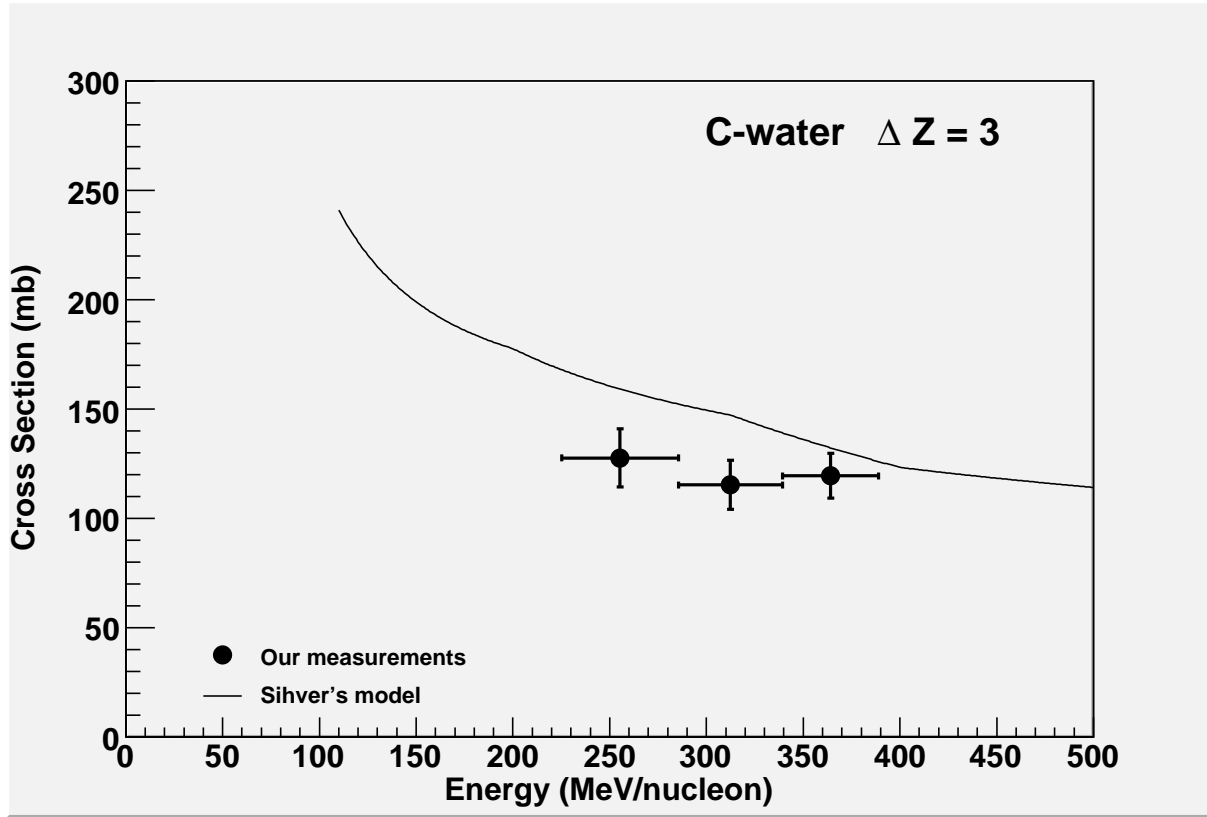


FIG. 10: Partial charge-changing cross sections of carbon-water interactions of  $\Delta Z = 3$  in comparison with a model calculation.

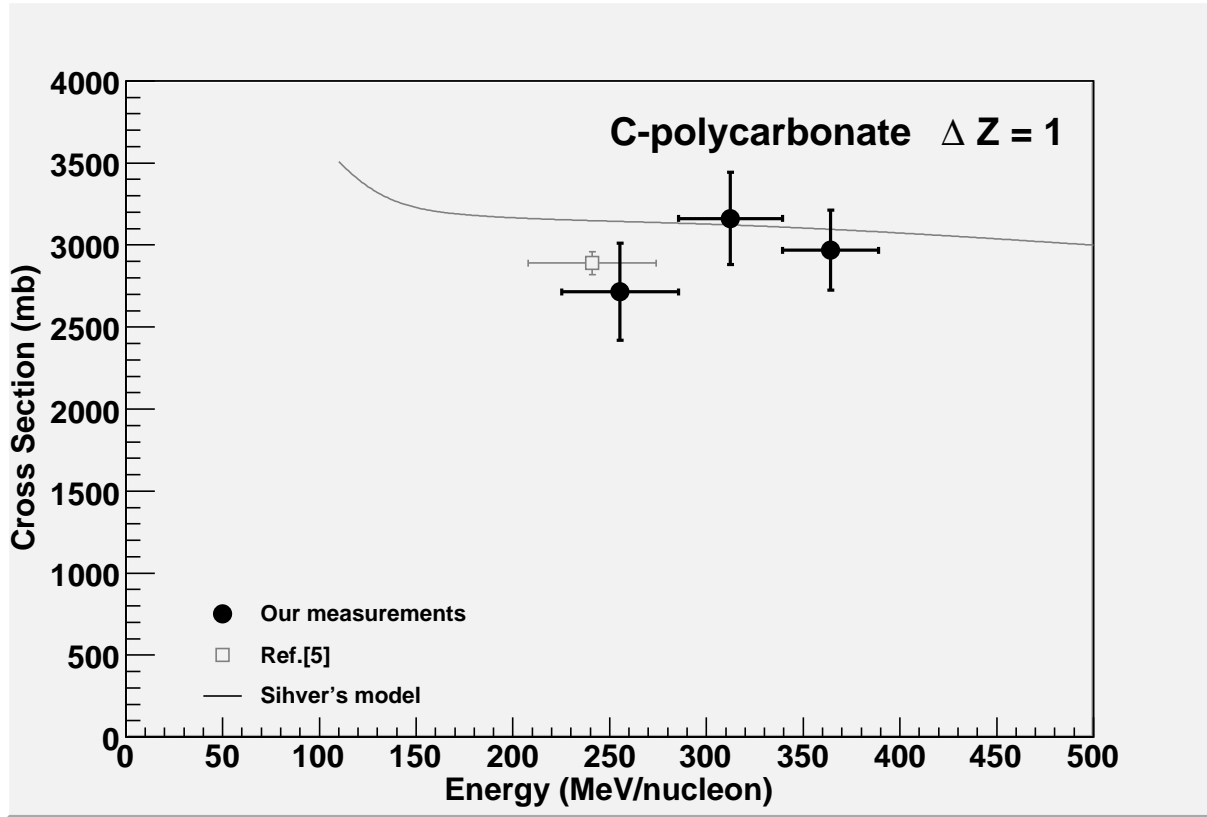


FIG. 11: Partial charge-changing cross sections of carbon-polycarbonate interactions of  $\Delta Z = 1$  in comparison with previous measurements and a model calculation.

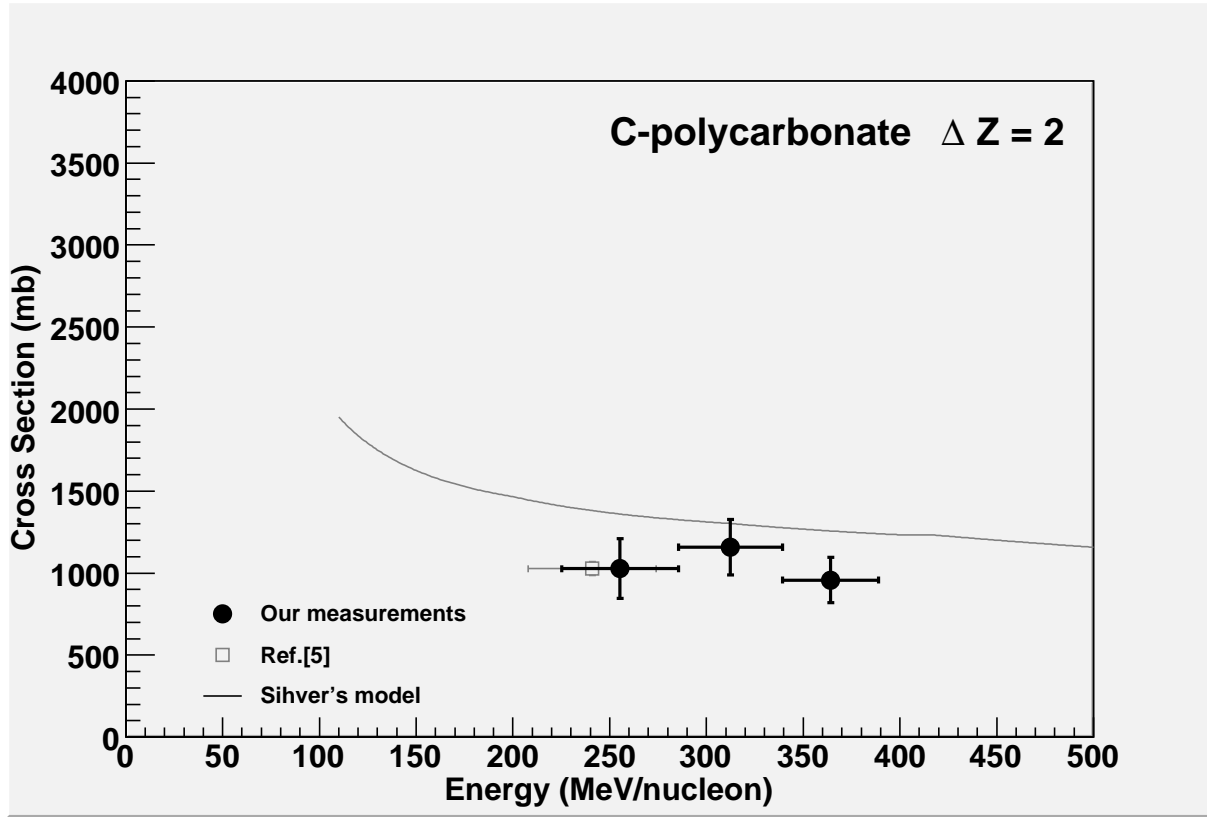


FIG. 12: Partial charge-changing cross sections of carbon-polycarbonate interactions of  $\Delta Z = 2$  in comparison with previous measurements and a model calculation.

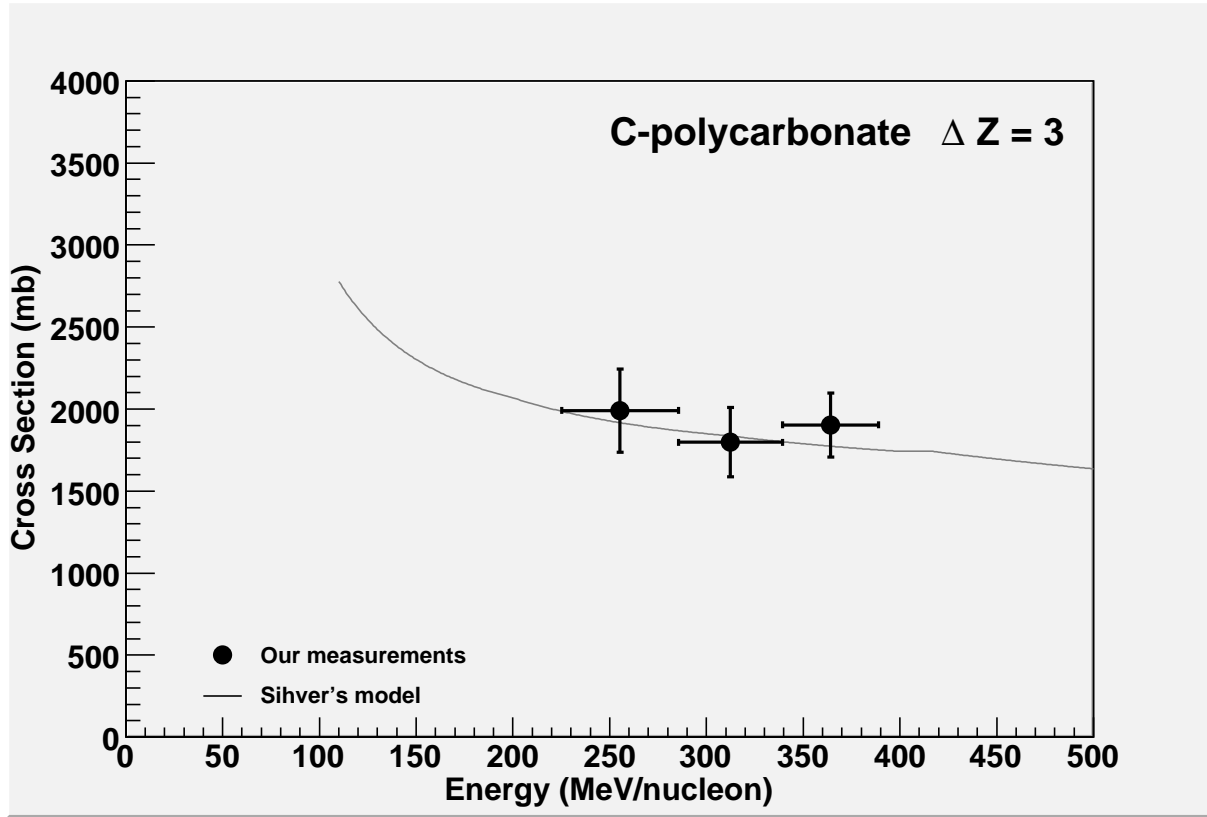


FIG. 13: Partial charge-changing cross sections of carbon-polycarbonate interactions of  $\Delta Z = 3$  in comparison with a model calculation.